Large-Scale Flow and Spiral Core Instability in Rayleigh-Bénard Convection

Igor Aranson[1], Michel Assenheimer[2], Victor Steinberg[3] and Lev S. Tsimring[4]

[1]*Department of Physics, Bar Ilan University, 52900 Ramat Gan, Israel*

[2]*Laboratoire de Physique Statistique, Ecole Normale Supérieure, 75231 Paris cedex 05, France*

[3]*Department of Physics of Complex Systems, The Weizmann Institute of Science, 76100 Rehovot, Israel*

[4]*Institute for Nonlinear Science, University of California at San Diego, San Diego, CA 92093-0402*

(February 9, 2008)

Abstract

The spiral core instability, observed in large aspect ratio Rayleigh-Bénard convection, is studied numerically in the framework of the Swift-Hohenberg equation coupled to a large-scale flow. It is shown that the instability leads to non-trivial core dynamics and is driven by the self-generated vorticity. Moreover, the recently reported transition from spirals to hexagons near the core is shown to occur only in the presence of a non-variational nonlinearity, and is triggered by the spiral core instability. Qualitative agreement between the simulations and the experiments is demonstrated.

PACS: 47.54+r, 47.20.Hw, 05.40.+j, 47.27.Te

One of the most intriguing and unexpected recent discoveries in natural pattern formation is the observation of spatio-temporally disordered spiral and target patterns [1,2] in large aspect ratio Rayleigh-Bénard convection (RBC) in Boussinesq fluids, in a parameter range where previously only rolls were known to be stable [3]. This regime is characterized by the spontaneous and continuous emergence and annihilation of large extended spiral and target patterns. Theoretically, these novel states were successfully reproduced both by numerical simulations of the Swift-Hohenberg (SH) model coupled to a self-consistent large-scale flow (see Eqs. 1-3) [4,5], as well as by the integration of the full thermally driven Navier-Stokes equations in the Boussinesq approximation [6]. It is currently postulated that the large-scale flow is necessary for the spatio-temporal chaotic state with many spirals and targets [4–7]. In a first attempt to understand these states, Cross and Tu proposed a physical mechanism based on wavenumber frustration, in which defects have an invasive nature and create spirals and targets [7]. In detailed experiments by Assenheimer and Steinberg [8,9], and more recently by Plapp and Bodenschatz [10], a new instability of spiral cores of single- and multi-armed spirals was observed. The striking feature of this instability is that spiral cores oscillate periodically with a frequency considerably higher than the frequency of the overall spiral rotation [10]. For yet higher supercriticality, a novel transition from spirals to hexagons was found in which both up- and downflow hexagons coexist [8,9]. These hexagons often invade the background RBC pattern, originating mainly from extended pattern cores.

In this Letter we present numerical simulations of the spiral core dynamics performed in the framework of the SH model coupled to a self-consistent large-scale flow. We show that this simple model exhibits both the spiral core instability and the spiral-to-hexagon transition, and that both are linked via the large-scale flow. In the case of the spiral core instability, we demonstrate that the velocity field generated by the spiral tip increases the local wavenumber and eventually drives the tip into the skew-varicose unstable region. Phase slips then occur, locally unwinding the spiral and returning the wavenumber into the stable domain. This instability is found to have a well-defined threshold in Rayleigh and Prandtl number space. Furthermore, the interpretation of the numerical results is supported by

the analysis of a similar but simpler problem: a single-armed spiral in an external velocity field created by a point vortex located at the spiral core, in the limit of infinite Prandtl number when the large-scale flow and the order parameter are decoupled. In addition, we observed, at higher supercriticality and only in the presence of non-variational nonlinear terms, a transition from spirals to hexagons. Both up- and downflow hexagons are generated simultaneously near the spiral core. In this scenario the core oscillations precede and trigger the transition to the hexagonal state.

We considered the well-established model, which describes RBC in a Boussinesq fluid rather successfully [11],

$$\psi_t + (\mathbf{u}\cdot\nabla)\psi = \epsilon\psi - g\psi^3 + 3(1-g)(\nabla\psi)^2\nabla^2\psi - \\ -(1+\nabla^2)^2\psi \tag{1}$$

$$\Omega_t - \sigma(\nabla^2 - c^2)\Omega = g_m\hat{z}\cdot\nabla(\nabla^2\psi)\times\nabla\psi \tag{2}$$

$$\Omega = \nabla\times\mathbf{u} \tag{3}$$

Here ψ is the order parameter, $\mathbf{u}$ the horizontal velocity field of the large-scale flow, and Ω the vertical component of the vorticity. The control parameter ϵ represents the reduced Rayleigh number, while σ characterizes the Prandtl number of the fluid. The parameter g allows to more accurately reproduce the stability properties of convection patterns, while g_m characterizes the coupling strength between the order parameter ψ and the vorticity Ω. The phenomenological parameter c is introduced to describe the local dissipation of the vorticity (e.g. due to friction at the bottom of the convection cell) [11,12]. Thus, Eq. 1 describes the dynamics of the order parameter ψ, while Eq. 2, using the definition of the vorticity (Eq. 3), represents the coupling of the large-scale flow field $\mathbf{u}$ and the order parameter. For $g = 1$ and $g_m = 0$ Eqs. 1-3 reduce to the Swift-Hohenberg equation (SHE).

We solved Eqs. 1-3 in a domain of 256×256 mesh points using a pseudo-spectral method based on the Fast Fourier Transform. The physical domain size was typically restricted to 150×150. Circular boundary conditions were enforced by ramping ϵ towards negative values at distances $r > R_{max} = 55$. The computations were performed on a parallel Cray J932

supercomputer, and verified on a 512×512 grid.

We started the simulations from initial conditions of the form $\psi = \cos(qr + n\theta)$, where r and θ are the polar coordinates, q is the wavenumber, and $n = \pm 1, \pm 2, \ldots$ is the topological charge of the spiral ($|n|$ is the number of spiral arms, while the sign corresponds to the chirality). These initial conditions relax in about 10 to 20 horizontal diffusion times to spirals. For sufficiently small values of the parameters ϵ and g_m (see Fig. 1), the spirals maintain a stable rigid rotation with an angular velocity depending both on g_m and ϵ, as well as on the topological charge n [13]. Typical spatial distributions of the order parameter and the vorticity field for one-armed spirals are shown, e.g. in Ref. [5]. As can be seen, the spiral tip generates a highly localized vorticity peak at the core. In the case of n-armed spirals, n identical vortices are created at the core. In this regime spiral cores are stable and only experience a slow off-center drift if the aspect ratio is not sufficiently large [12].

For ϵ above some threshold, depending on g_m (see Fig. 1), we observed a novel spiral core instability. In contrast to the off-center drift, it persists even in an infinite system, since the unstable mode is localized near the core. The main feature of the instability is that the spiral core oscillates in the reference frame of the rotating spiral. The amplitude of the modulation, caused by the core oscillation, increases from zero as the bifurcaton is crossed towards higher values of ϵ and g_m. The critical value of the control parameter ϵ depends on g_m as well as on n. Figure 1 shows the bifurcation diagram as a function of ϵ and g_m for $n = 1, 2$ [13]. Figure 2 presents typical numerical as well as experimental snapshots of the core oscillation for one-armed spirals [14]. Similar behavior occurs for two-armed spirals.

The core oscillations can be illustrated by comparing the temporal behavior of the order parameter at points near the core and at the rim. At the edge, the core oscillations are negligible so that mainly the background rotation is sensed. Figure 3 shows plots for one-armed spirals for three values of ϵ. Figure 3(a) illustrates the rigid spiral rotation, below the threshold for core oscillations. The central (solid line) and peripheral points (dashed line) oscillate with the same frequency, the unambiguous signature of the spiral's rigid rotation. Figures 3(b) and 3(c) show the spiral dynamics above criticality. Here, the core oscillates

at a much higher frequency than the peripheral point. The core thus has a fast rotation in the framework of the spiral's overall rotation.

The corresponding experimental data are shown in Fig. 4. Figure 4(a) shows the rigid body rotation of a one-armed spiral below the onset of the core instability. Clearly, the oscillations near and away from the core are phase-locked. Figure 4(b) presents the fast oscillations of the core above the threshold of the instability. On this short time scale the peripheral signal does not vary significantly and is not shown. Similar dynamics were reported in Refs. [8,10].

Our numerical simulations of the full model (Eqs. 1-3) suggest that the vorticity generated by the spiral tip plays a major role in the core dynamics. Therefore, the origin of the core oscillations can easily be understood - at least qualitatively - in the framework of the following simplified model. Consider a one-armed spiral solution of the form $A(r)\cos\phi$, where $\phi = qr + \theta$, in the framework of the SHE (Eq. 1), coupled to an external velocity field generated by a fixed point vortex with circulation Γ, placed at the center of rotation. The sign of the vortex is chosen to correspond to the self-generated vortex in the full model. Using the phase approximation (i.e. neglecting the variations of the amplitude $A(r)$), we obtain (see Refs. [12,15]), that $\phi_t = \Gamma/r^2\partial_\theta\phi + \dots$. Therefore, the local wavenumber increases linearly, $q_t \propto \Gamma/r^2$. In other words, the external velocity field winds the spiral up near the core. Eventually, the local wavenumber will be carried away from the stable band and the skew-varicose (or Eckhaus) instability will be initiated. This stage can no longer be described within the phase approximation. Abrupt phase jumps by 2π (phase slips) consequently emerge and return the wavenumber back into the stable region. This process then recurs, leading to quasi-periodic oscillations.

We simulated the spiral dynamics using this simplified model, with a velocity profile of the form $\mathbf{u} = \Gamma r^{-1}\hat{\theta}$, and observed the abovementioned scenario. As the magnitude of the circulation Γ increases, a bifurcation similar to the one described above occurs. At small Γ a steady rotation persists, while for $\Gamma > \Gamma_c$ the core starts to oscillate. Interesting dynamics also develop if the sign of the external circulation and the spiral-generated vortex

are opposite. Then, the local velocity field unwinds the spiral, driving it into the zig-zag unstable region [16]. Because it is non-local, this instability cannot be saturated by phase slips and eventually destroys the spiral. This might occur when a spiral is driven by the external vorticity created by another oppositely charged spiral and could be relevant for the persistence of the spiral turbulent state [1,2].

Recently Assenheimer and Steinberg reported a transition from the spiral and target chaotic state to a state of up- and downflow hexagons, as the supecriticality ϵ increased [9]. These hexagons started to develop and invade the system primarily from spiral and target cores and other defects. Dewel et al. [17] demonstrated that in the framework of the SHE at large ϵ, the coexistence and linear stability of up- and downflow hexagons is caused by the excitation of a *quasineutral* zero mode, which breaks the inversion symmetry $\psi \to -\psi$. Despite their linear stability, these hexagons are nonlinearly unstable because their free energy, in the framework of the pure variational SHE ($g = 1$, $g_m = 0$), is higher than that of rolls. As a result, nuclei of hexagons, immersed in rolls, ultimately shrink. Because the generalized SHE (Eq. 1-3) with either $g \neq 1$ and/or $g_m \neq 0$ is non-variational, a simple relative stability analysis of rolls versus hexagons becomes impossible.

Numerics performed with a non-variational coefficient $1 - g = 0.25$, relatively large coupling to the vorticity $g_m = 10$ (customary for this model, e.g. Ref. [12]) and supercriticality above the threshold for the spiral core instability, $\epsilon = 1.9$, show that hexagons indeed invade rolls. We have observed the simultaneous nucleation of up- and downflow hexagons at the core which subsequently spread out (see Fig. 5). Similar dynamics, obtained experimentally, is shown in Fig. 6. However, one might speculate that a local wavenumber change near the core, rather than the large-scale flow, causes the transition. To compare, we performed simulations for the same parameters but without a large-scale flow (i.e. $g = 0.75$, $g_m = 0$ and $\epsilon = 1.9$). In this case spots emerge from the side wall rather than from the core region. It is thus plausible to suggest that the large-scale flow, arising primarily near spiral cores and other defects, generates the zero mode of the order parameter [18]. Thus, the spiral core instability initiates the nucleation of hexagons. Since the $\psi \to -\psi$ symmetry is still

preserved, both up- and downflow hexagons nucleate simultaneously.

Summarizing, we studied effects of large-scale flow on the dynamics of a spiral core. Although our computations were performed in the framework of a simplified phenomenological model, two characteristic features of the dynamics were found also observed experimentally: the spiral core instability and the spiral-to-hexagon transition. The vorticity field generated at a spiral core when $g_m \neq 0$, plays a major role in the spiral oscillations. These oscillations are not observed in the variational model in which the coupling with the vorticity mode is absent (i.e. $g_m = 0$). On the other hand, very similar oscillations are observed in a model with a fixed vortex pinned at the center of rotation of the spiral. At higher supercriticality the vorticity drives the zero-mode of the order parameter ψ and prompts the hexagon formation. In that case, the core oscillations initiate the transition to the hexagonal state. Certainly, a more detailed analysis of a physically more justified (but more complicated) model, similar to that of Ref. [6], is desirable.

I.A. was supported by the Raschi Foundation and Israeli Science Foundation. M.A. benefitted from a Human Capital and Mobility Fellowship. L.T. was supported by the U.S. Department of Energy and acknowledges the hospitality of Bar Ilan University and The Weizmann Institute of Science. Support by the Minerva Center for Nonlinear Physics of Complex Systems and the Inter-Israeli Center for Supercomputing is also acknowledged.

REFERENCES

[1] M. Assenheimer and V. Steinberg, Phys. Rev. Lett. **70**, 3888 (1993); Nature, **367**, 345 (1994).

[2] S. W. Moris, E. Bodenschatz, D.S. Cannel and G. Ahlers, Phys. Rev. Lett. **71**, 2026 (1993).

[3] F.H. Busse, J. Fluid Mech. **30**, 625 (1967); Rep. Prog. Phys. **41**, 1929 (1978).

[4] H. Xi, J.D. Gunton, and J. Viñals, Phys. Rev. E **47**, R2987 (1993)

[5] M. Bestehorn, M. Frantz, R. Friedrich, and H. Haken, Phys. Lett. A. **174**, 48 (1993).

[6] W. Decker, W. Pesch, and A. Weber, Phys. Rev. Lett. **73**, 648 (1994).

[7] M.C. Cross and Y. Tu, Phys. Rev. Lett. **75**, 834 (1995).

[8] M. Assenheimer, Ph. D. thesis, The Weizmann Institute of Science, 1994.

[9] M. Assenheimer and V. Steinberg, Phys. Rev. Lett. **76**, 756 (1996); to be published.

[10] B. B. Plapp and E. Bodenschatz, Core Dynamics of Multi-Armed Spirals in Rayleigh-Bénard Convection, submitted to Physica Scripta (1996).

[11] H. S. Greenside and M. C. Cross, Phys. Rev. A **31**, 2492 (1985).

[12] M. Cross and P.C. Hohenberg, Rev. Mod. Phys. **65**, 851 (1993).

[13] At even smaller g_m spirals undergo a spontaneous transition to targets via a core reconnection and expulsion of emerging dislocations off to the boundary (see Ref. [1]).

[14] The experimental data depicts the optical intensity of the shadowgraph signal, related to the order parameter ψ.

[15] M.C. Cross and A. C. Newell, Physica D **10**, 299 (1984).

[16] In this simplified model the Prandtl number is infinite. Then, the first instability for

$q < q_c$ is zig-zag [12].

[17] G. Dewel, S. Métens, M'F. Hilali, P. Borckmans, and C.B. Price, Phys. Rev. Lett. **74**, 4647, (1995).

[18] Large-scale flow and zero mode of the order parameter should not be equated. Physically, the latter can be related to the long-wave variation of the vertical temperature gradient from its nominal value. Note, while the zero mode has different signs for up- and downflow hexagons, the vertical vorticity has the same sign everywhere.

FIGURES

FIG. 1. Stability diagram for one- (a) and two-armed (b) spirals for $c^2 = 2$, $\sigma = 1$ and $g = 1$. As ϵ increases, the spiral core becomes unstable at the dashed line, regaining stability at the solid line as ϵ decreases.

FIG. 2. Snapshots of periodic spiral core oscillations. Top row: simulations with $\epsilon = 1.45, g = 0.9, g_m = 27, c^2 = 2$ and $\sigma = 1$; time delay between frames 5, and integration domain radius $R = 55$. Bottom row: experiments with $\epsilon = 2.88$ and $\sigma = 4.5$.

FIG. 3. Order parameter ψ at the core (solid) and periphery (dashed) of a one-armed spiral with $g = 1, g_m = 95, \sigma = 5$ and $c^2 = 1$: (a) below threshold ($\epsilon = 1.1$); (b),(c) above threshold ($\epsilon = 1.3$ and 1.35).

FIG. 4. Shadowgraph intensity at the core (solid) and periphery (dashed) of a one-armed spiral: (a) below threshold ($\epsilon = 2.05, \sigma = 4.5$) and (b) above threshold ($\epsilon = 2.88, \sigma = 4.5$). In (b) only the fast core signal is shown.

FIG. 5. Hexagon invasion from a spiral core obtained from the full model with $\epsilon = 1.9, g = 0.75, g_m = 10, c^2 = 2$ and $\sigma = 1$. Snapshots taken at $t = 10, 110, 470, 650, 340, 2350$.

FIG. 6. Experimental hexagon nucleation at a spiral core with $\epsilon = 3.19$, $\sigma = 4.5$ and time delay between frames $\Delta t = 3.6$, 3.6, 22.7, 18.0, 10.7 τ_v.

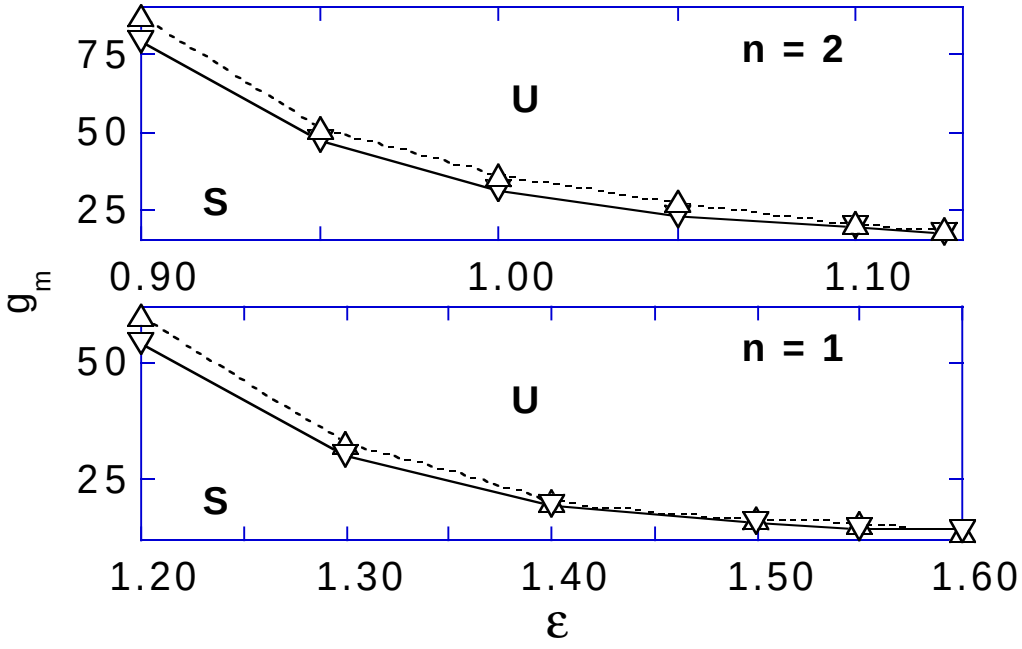

I. Aranson, M. Assenheimer, V. Steinberg, L. S. Tsimring
Large-Scale Flow and Spiral Core Instability in Rayleigh-Benard Convection

Figure 1

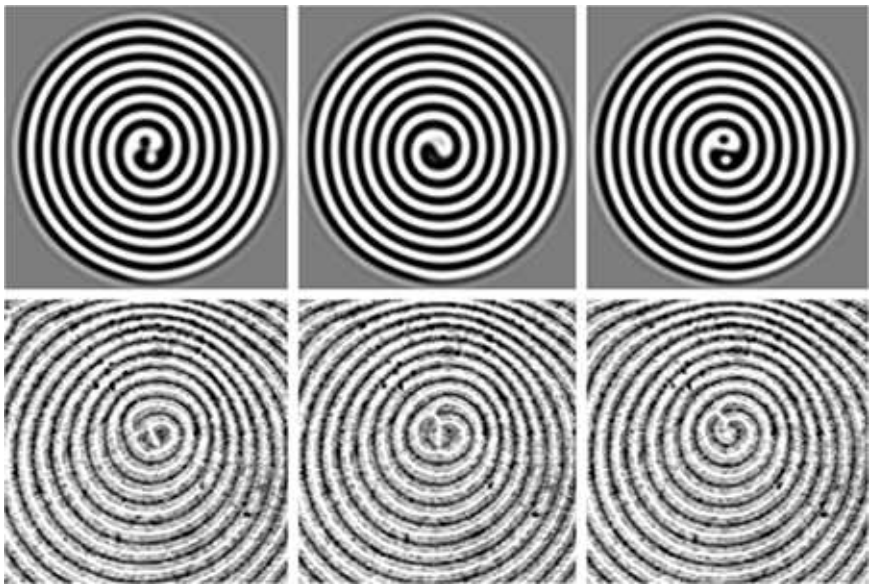

I. Aranson, M. Assenheimer, V. Steinberg, L. S. Tsimring
"Large-Scale Flow and Spiral Core Instability in Rayleigh-Bénard Convection"

Figure 2

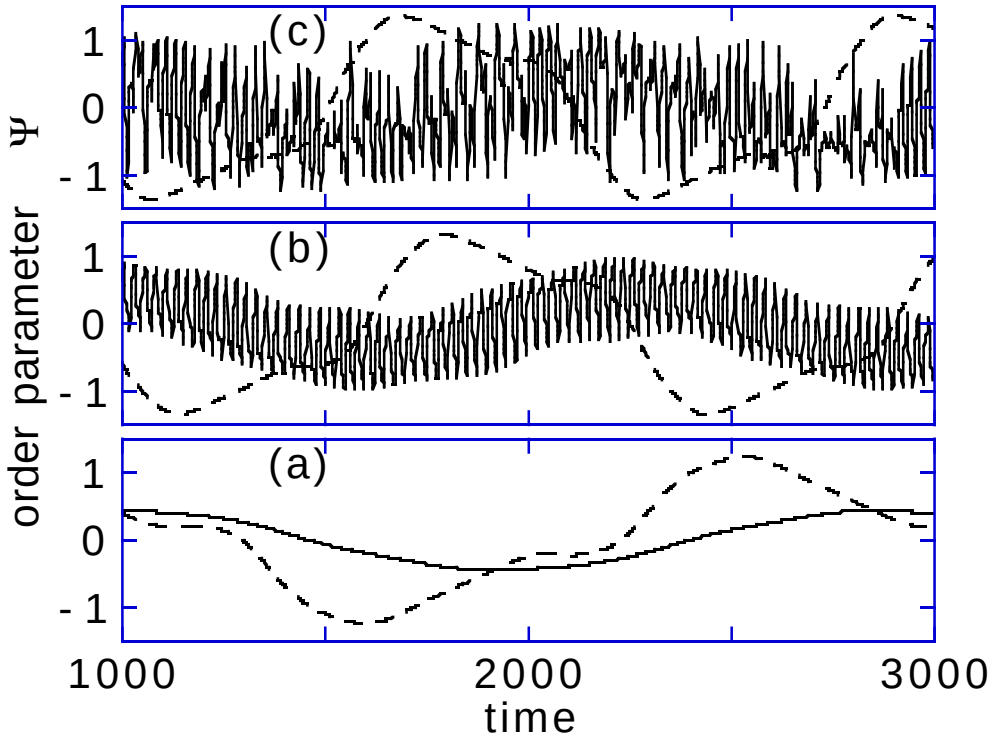

I. Aranson, M. Assenheimer, V. Steinberg, L. S. Tsimring
Large-Scale Flow and Spiral Core Instability in Rayleigh-Benard Convection

Figure 3

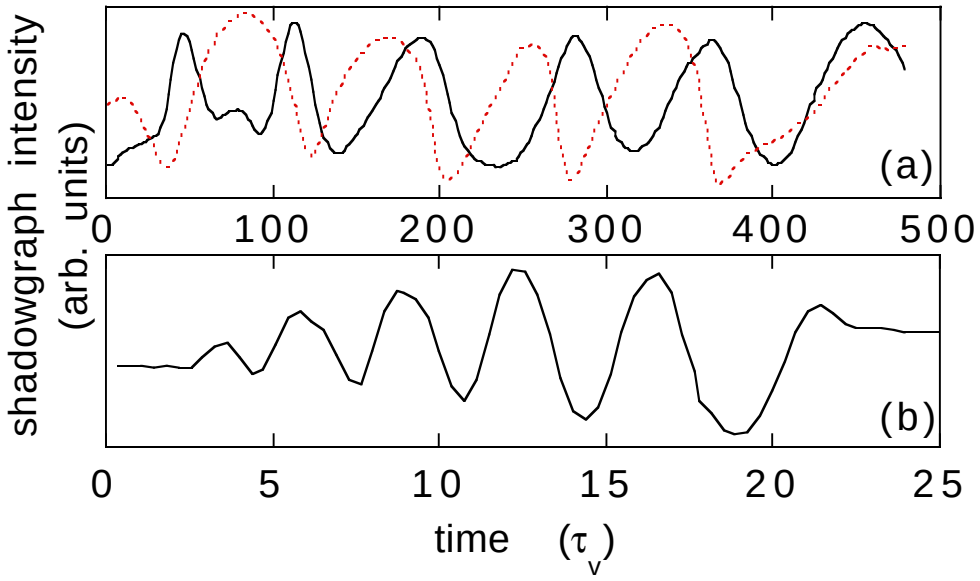

I. Aranson, M. Assenheimer, V. Steinberg, L. S. Tsimring
Large-Scale Flow and Spiral Core Instability in Rayleigh-Benard Convection

Figure 4

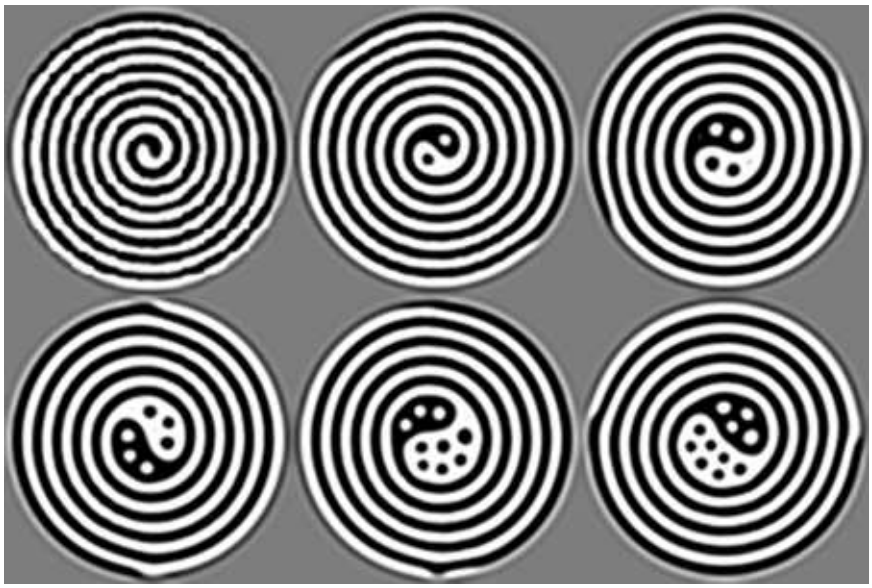

I. Aranson, M. Assenheimer, V. Steinberg, L. S. Tsimring
"Large-Scale Flow and Spiral Core Instability in Rayleigh-Bénard Convection"

Figure 5

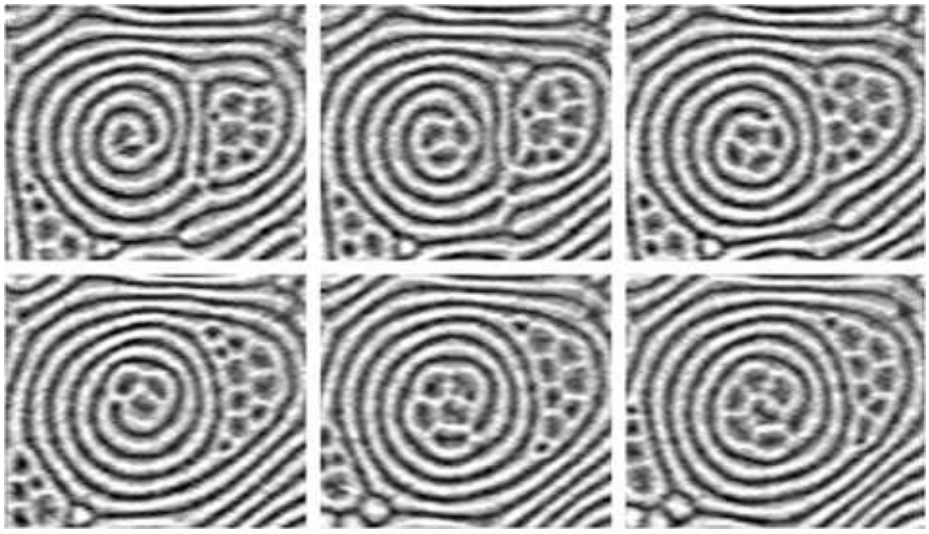

I. Aranson, M. Assenheimer, V. Steinberg, L. S. Tsimring
"Large-Scale Flow and Spiral Core Instability in Rayleigh-Bénard Convection"

Figure 6